LANGMUIR

pubs.acs.org/Langmuir Article

Scalable Synthesis of Planar Macroscopic Lipid-Based Multi-Compartment Structures

Richard J. Archer,* Shogo Hamada, Ryo Shimizu, and Shin-Ichiro M. Nomura*

Cite This: *Langmuir* 2023, 39, 4863−4871 Read Online

ACCESS | Metrics & More | Article Recommendations | Supporting Information

ABSTRACT: As life evolved, the path from simple single cell organisms to multicellular enabled increasingly complex functionalities. The spatial separation of reactions at the micron scale achieved by cellular structures allowed diverse and scalable implementation in biomolecular systems. Mimicking such spatially separated domains in a scalable approach could open a route to creating synthetic cell-like structured systems. Here, we report a facile and scalable method to create multicellular-like, multi-compartment (MC) structures. Aqueous droplet-based compartments ranging from 50 to 400 μm were stabilized and connected together by hydrophobic layers composed of phospholipids and an emulsifier. Planar centimeter-scale MC structures were formed by droplet deposition on a water interface. Further, the resulting macroscopic shapes were shown to be achieved by spatially controlled deposition. To demonstrate configurability and potential versatility, MC assemblies of both homogeneous and mixed compartment types were shown. Notably, magnetically heterogeneous systems were achieved by the inclusion of magnetic nanoparticles in defined sections. Such structures demonstrated actuated motion with structurally imparted directionality. These novel and functionalized structures exemplify a route toward future applications including compartmentally assembled "multicellular" molecular robots.

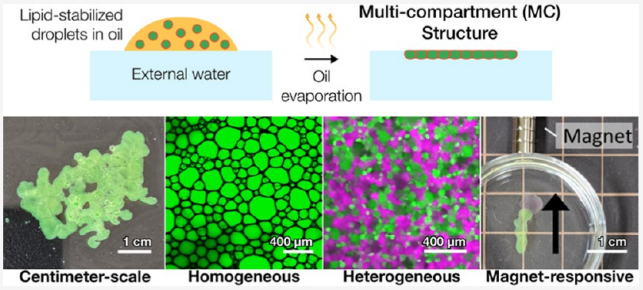

INTRODUCTION

In nature, the evolution of a single cell to multicellular organisms was a significant step toward increasingly complex forms of life.[1−3] This change from the unicellular form, where all living functions must occur in the same shared space, to the spatially separated compartmentalized structures of multicellular life allowed for specialization, optimization, and synergy of biochemical processes to develop.[4−7] The advantages in such physical divisions are apparent in biological systems where cell specialization has led to the development of tissues and organs, which leads to the whole becoming greater than the sum of its parts.[8−10] This cellular approach to building larger-scale materials from assembled smaller units is also being investigated for producing synthetic "multi-compartment" (MC) structures.

Lipid-based structures such as giant unilamellar vesicles are often studied as synthetic analogues to biological cells in terms of their size, membrane structure, and composition and their ability to encapsulate solutions.[11−15] Several studies have already shown an interesting array of lipid-based biomimetic functionality including enhanced diffusion,[16−18] lipid self-replication,[19] and stimulated morphological changes;[20,21] however these studies have so far focused on the unbound "unicellular" structures, limiting their overall functionality.

There has been a recent growing interest in assembling liposomes into connected "multicellular"-like MC structures to expand their functionalities.[22−26] Reported strategies to achieve MC lipid-based structures have included microfluidic assemblies,[27] spontaneous assemblies,[28] electrostatic interactions,[29,30] manual manipulation by optical traps,[31] and through emulsion phase transfer by allowing lipid-stabilized emulsion droplets to self-concentrate by settling at the interphase before transfer.[32] Separately, MC structures have also been formed as "droplet networks", whereby lipid stabilized aqueous droplets are connected together by hemi-fusion inside an external oil phase by simple proximity and without coalescence. While serving as interesting models, their requirement for an external oil phase limits their practical utility.[33−36] A small number of studies have begun to utilize such MC structures by connecting different mono-functional compartments together, and a greater group functionality was achieved.[37,38] These studies have so far been limited in size and complexity due to the difficulties in easily producing large MC structures, especially with a directed assembly. To address such limitations, our group have previously shown a new simple method to form MC lipid-based structures from lipid-soaked sponges in the

Received: October 19, 2022
Revised: February 28, 2023
Published: March 28, 2023

https://doi.org/10.1021/acs.langmuir.2c02859
Langmuir 2023, 39, 4863−4871

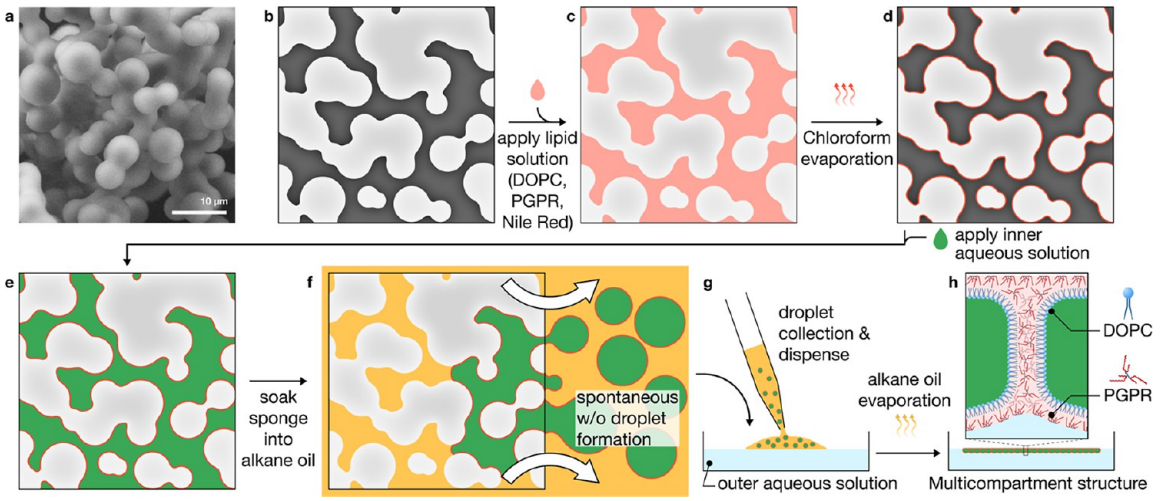

Figure 1. Schematic representing the basic procedure to achieve lipid-based MC assemblies. (a) SEM image of MG sponge, (b) schematic of MG sponge, (c) MG sponge is soaked with a chloroform based lipid solution (red), (d) the chloroform carrier of the lipid solution is then allowed to evaporate, (e) dried MG sponges with deposited lipids can then be soaked with an aqueous solution (green), (f) aqueous solution-soaked MG–lipid sponges can be placed into an oil phase (orange), which causes the aqueous phase to be spontaneously expelled as stabilized droplets as the MG sponge favorably absorbs the oil, (g) the expelled aqueous droplets can be pipetted out of the solution onto the surface of an external aqueous phase (blue), (h) the external oil is allowed to evaporate, and (h) the aqueous droplets then assemble together into a MC structure floating as a planar layer on an aqueous interface.

millimeter range.[39] While this work paved the way toward practical large-scale MC assemblies, there were still limitations in the overall size, due to which we could only form connections of one compartment type and direct controllability in the resulting structure was not possible. Here, we present a drastic improvement in the formation of MC lipid-based structures into the centimeter range. Additionally, we show the ability to control the compartment spatial organization, the ability to connect compartments of different types for heterogeneity, and the inclusion of responsive particles to extend functionality. The method demonstrated here can be done easily and without the need for any specialized equipment. These lipids-based MC structures consisting of biocompatible components show good stability and longevity with tailorability and the capability to efficiently encapsulate hydrophilic molecules as well as accommodate hydrophobic species between compartments. The compartment assembly can be produced from different droplet types in a heterogeneous assembly, increasing their potential versatility. The addition of magnetic nanoparticles allows for easy external actuation of the MC structures, combined with the heterogeneous assembly of magnetic and non-magnetic sections, and a directionality to the induced motion was observed.

MATERIALS AND METHODS

Dimethyldimethoxysilane (DMDMS, 95%), methyltrimethoxysilane (MTMS, 98%), iron(ii) sulfate hydrate (99%), iron(iii) sulfate hydrate (97%), ammonia (28–30%), and oleic acid (90%) were purchased from Merck Sigma-Aldrich, Inc., Germany. Nile red fluorescent red dye, hexane (96%), hexadecane (97%), and chloroform (99%) were purchased from Wako Pure Chemical Industries, Ltd., Japan. 1,2-Dioleoyl-*sn*-glycero-3-phosphocholine (DOPC) was purchased from NOF CORPORATION (NOF), Japan. Urea (99%) was purchased from Nacalai Tesque Inc. Japan.; cetyltrimethylammonium chloride (CTAC, 95%) was obtained from Tokyo Chemical Industry, Ltd.; and polyglycerol-polyricinorate (PGPR), Poem-100, was purchased from RIKEN Vitamin, Japan. Calcein fluorescent green dye was purchased from DOJINDO Laboratories, Inc. Japan. Dextran, Texas Red 40,000 MW was purchased from Thermo Fisher Scientific. α-Hemolysin was purchased from List Biological Labs, Inc, USA. Phosphate buffered saline was obtained from OXOID, Ltd., UK. All reagents were used as received.

MG Sponge Formation. Silicone-based "marshmallow-like" sponges, hereafter referred to as MG sponges, were prepared in a sol–gel process as previously reported.[40] Briefly, a sol solution was prepared by adding acetic acid (5 mM) to CTAC and urea, and the solution was stirred until completely dissolved. A mixture of DMDMS and MTMS (2:3) was added quickly to the CTAC solution. The final concentrations were as follows: acetic acid 5 mM, urea 0.25 g/mL, CTAC 0.05 g/mL, MTMS 0.15 mL/mL, and DMDMS 0.1 mL/mL. The solution was stirred for 30 min before it was placed in a sealed container and left in an oven at 80 °C overnight to promote gelation. The resulting gel was carefully removed from the container and washed with repeated cycles of water and ethanol to remove CTAC and urea.

MG Sponge Loading. Prepared blank MG sponges [scanning electron microscopy (SEM) image of the MG sponge structure Figure 1a and schematic of the structure Figure 1b] were first infused with a lipid solution containing concentrations of DOPC, PGPR, and Nile red dissolved in chloroform, and the solution was pipetted directly on the sponge, which would rapidly swell until saturated and approximately 100 μL of lipid solution was used per 1 cm^3 sponge (Figure 1c). Lipid-soaked sponges would then be allowed to dry at room temperature overnight (Figure 1d). Lipid–MG sponges could then be saturated with an aqueous liquid, again by simple pipetting the desired aqueous solution onto the sponge. Water-based solutions were slowly absorbed by lipid–MG sponges over 5 min until the sponge was saturated (Figure 1e), and unlike with chloroform solutions, saturation of the sponge using aqueous solutions did not cause swelling. Aqueous solution-saturated lipid–MG sponges were placed in alkane oils such as hexane, decane, and hexadecane, resulting in the formation of aqueous droplets being ejected from the MG sponge as the oil preferentially entered, causing displacement (Figure 1f). After 30–60 s, the displacement was visibly complete, and the MG sponges were removed. Droplet collection was achieved by simple manipulation using a micropipette with a pipette tip with an opening wider than the diameter of droplets (Figure 1f); in some cases, the tapered pipette tips were cut shorter to produce a wider opening. Withdrawing aqueous droplets inevitably also drew up excess oil. Due to the greater density of water, the droplets would sediment

https://doi.org/10.1021/acs.langmuir.2c02859
Langmuir 2023, 39, 4863–4871

and self-accumulate in the pipette tip, and the high concentration of droplets could then be gently expelled from the pipette onto the surface of an external aqueous solution (Figure 1g). In cases where volatile oils were used, the evaporation caused the droplets stabilized by lipids and PGPR to pull together into lipid-based hemi-fused MC structures on the surface of an external aqueous solution (Figure 1h).

Superparamagnetic Iron Oxide Nanoparticle Synthesis. Superparamagnetic iron oxide nanoparticles (SPIONs) were synthesized using the well-established co-precipitation method.[41] Briefly, iron(ii) sulfate and iron(iii) sulfate were dissolved in water in a 1:2 molar ratio and subsequently co-precipitated by ammonia hydroxide (28−30 wt %) under an oxygen-free environment. To achieve the oxygen-free environment, solutions were vigorously bubbled with argon gas for 30 min before use, and a stream of argon gas was also passed over during the reaction to prevent influx of oxygen.

Instruments. Microscopy analysis was performed using an Olympus IX71 microscope with an attached Hamamatsu Orca Spark camera. Images were taken at a resolution of 900 × 600 pixels. Confocal microscopy was performed using either an Olympus FV-1500 or a Zeiss LSM980. Vortexing was performed using a Vortex Genie 2.

RESULTS AND DISCUSSION

MG silicone sponges prepared by the polymerization of methyl trimethoxysilane and dimethyl dimethoxysilane were easily produced using the protocol outlined in the Materials and Methods section. The resulting MG sponge was soft and easy to cut, had a low density of approximately 0.15 g cm^{-3}, and acted as a suitable support structure to the DOPC lipid and hydrophobic PGPR surfactant. Blank MG sponges before the addition of lipids were completely hydrophobic and could not absorb any water into the matrix. The addition of PGPR and/or DOPC onto the MG sponge allowed the slow absorption of water into the sponge matrix. Increasing the amount of DOPC adsorbed on the sponge surface resulted in faster and greater absorption of water into the matrix, while increasing the amount of adsorbed PGPR resulted in slower and less absorption of water into the matrix. As both DOPC and PGPR allow the absorption of water into the sponge matrix, it is likely that both chemicals play a role in stabilizing the subsequent aqueous droplets.

Using the procedure described in the Materials and Methods section (with DOPC, PGPR, and oil hexadecane concentration sets at 3.25 mM, 5 wt %, and 0.5 vol % respectively), a large ∼2 × 4 cm macroscopic MC lipid-based structure was assembled on an external aqueous environment from the combined droplets of six lipid and buffer soaked 5 × 5 mm MG sponges totaling a combined volume of approximately 300 μL aqueous internal volume (Figure 2a). The resulting structure was observed by phase contrast optical microscopy to qualitatively assess the compartment shapes and sizes (Figure 2b). The initial droplets appeared to be connected together with a distorted, non-spherical shape as it took a tightly packed formation. The compartmental, separated structure of the lipid stabilized droplet network remained intact after the loss of the external hexane oil with no observed compartment coalescence occurring in the observation period, and the compartment size distribution was found to be 50−400 μm. Confocal microscopy was used to observe the encapsulation of both hydrophilic and hydrophobic dyes. Green fluorescence correlating to the hydrophilic dye (calcein) was found to be localized only to the inside of the individual compartments, confirming high aqueous phase encapsulation efficiency (Figure 2c). A red fluorescent hydrophobic dye (Nile red) was found to be surrounding the hydrophilic compartments in a continuous network, believed to indicate the lipid−PGPR rich phase (Figure 2d). The external aqueous media did not show any observable discoloration caused by leaking compartments over 1 week, indicating a high level of stability for lipid-based structures over this time period.

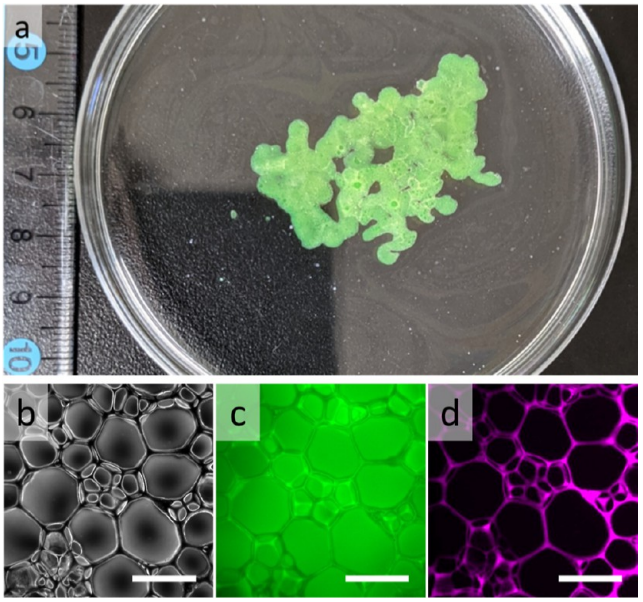

Figure 2. (a) Centimeter scale (∼2 × 4 cm) MC structure floating on top of water with a standard ruler for size comparison, image taken by a smartphone camera; (b) phase contrast image; (c) green fluorescence image showing the location of hydrophilic calcein dye; and (d) purple fluorescence image showing the location of hydrophobic Nile red dye in the lipid membrane. No significant difference was observed when MCs were made without internal dye (Figure S1). Images (b−d) scale bar 400 μm.

Experiments were performed to determine the required and optimal conditions for the lipid-based solution used to coat the MG sponges. The importance of both PGPR and DOPC was assessed by combining the two in different ratios in the lipid solution added to the MG sponge. Figure 3 gives examples of the resulting structures, where calcein fluorescent dye was added to the internal aqueous phase to identify the encapsulation. When the lipid solution contained a concentration of DOPC at 32.0 mM, the resulting structures were typically highly fragmented, and combined with PGPR at 2.5 wt %, relatively few compartments were formed (Figure 3a). Increasing the PGPR concentration to 5.0 wt % improved the number of lipid compartments formed, but the structures were poorly defined with additional lipid build-up on the surface (Figure 3b). At a PGPR concentration of 10.0 wt %, the lipid structures were better defined than those prepared at lower PGPR concentrations but showed excess build-up at the boundaries of the lipid compartments; additionally, green fluorescence emission in the lipid layers was extremely bright even compared to that of the aqueous compartments, indicating the presence of hydrophilic calcein dye within the hydrophobic outer layer, which is not observed in systems with lower lipid concentrations. PGPR may therefore accommodate the calcein dye into the lipid layer, an unwanted effect (Figure 3c). Lowering the concentration of DOPC in the lipid solution to 3.25 mM resulted in clearer and well-defined MC structures at PGPR concentrations of 2.5 wt % and 5.0 wt % (Figure 3d,e respectively). A PGPR concentration of 5.0 wt % showed a

https://doi.org/10.1021/acs.langmuir.2c02859
Langmuir 2023, 39, 4863−4871

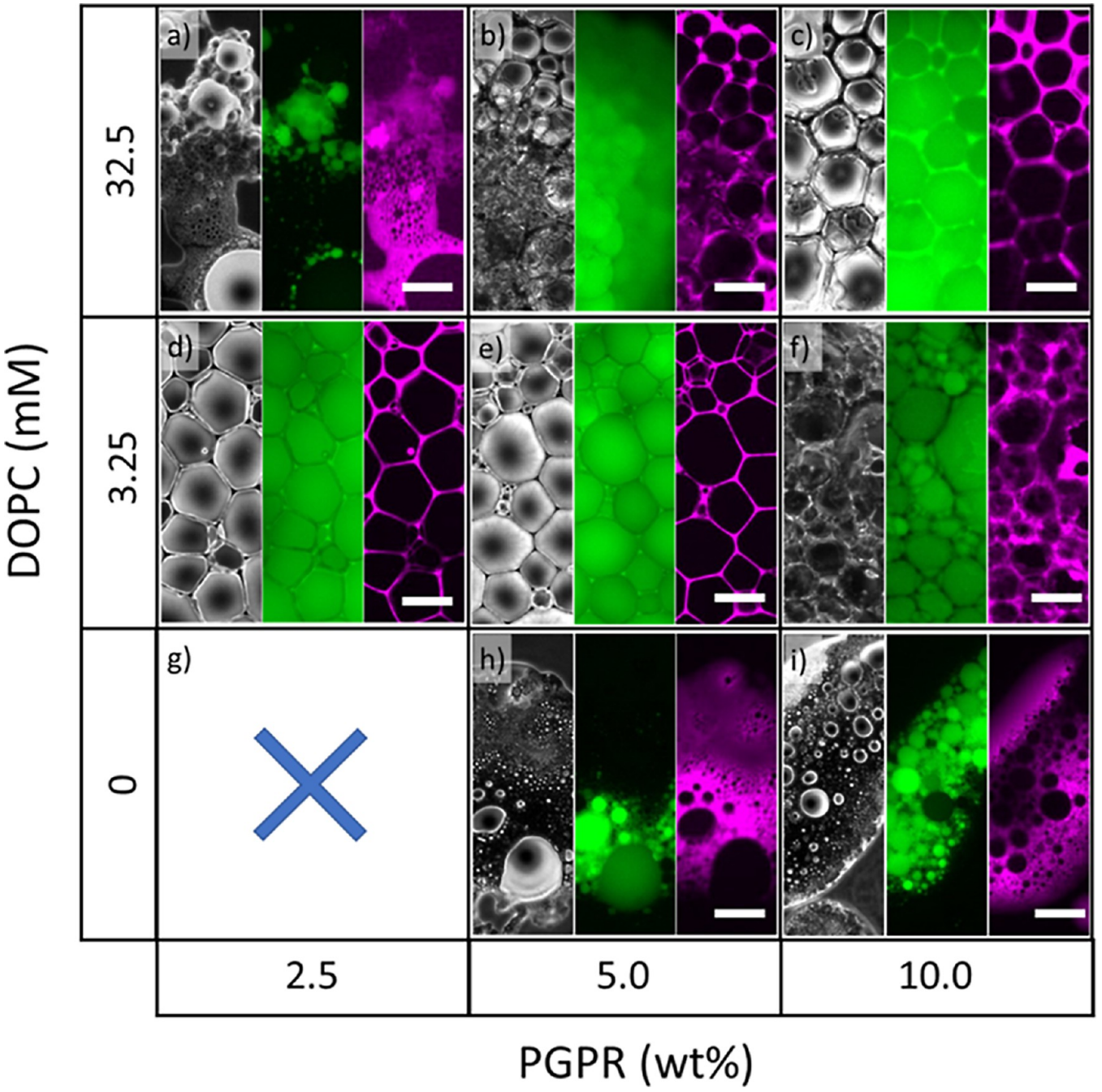

Figure 3. Microscopy phase contrast images of representative structures formed by various concentrations of DOPC and PGPR with fluorescence images of the same area at a DOPC concentration of 32.5 mM and PGPR concentrations of 2.5, 5.0, and 10.0 wt % (a−c), respectively. DOPC concentration of 3.25 mM and PGPR concentrations of 2.5, 5.0, and 10.0 wt % (d−f), respectively. A DOPC concentration of 0 mM and 2.5 wt % PGPR did not show any encapsulation (g) and a DOPC concentration of 0 mM and PGPR concentrations of 5.0 and 10.0 wt % shows amorphous structures (h,i, respectively). Scale bar 400 μm.

moderate increase in stability over that of a PGPR concentration of 2.5 wt % as the structures remained intact for longer before starting to break apart (2 vs 1 h respectively). At a DOPC concentration of 3.25 mM and a PGPR concentration of 10.0 wt %, the structures formed stable MC structures; however, the phase contrast imaging showed a large oily build-up surrounding the compartments, and green fluorescence showed a greater distance between compartments (Figure 3f). To demonstrate the role of DOPC, samples were prepared using only PGPR. With DOPC at 0 mM and PGPR at 2.5 wt %, no structures or encapsulation of inner aqueous solution was observed (Figure 3g). At a DOPC concentration of 0 mM and PGPR concentrations of 5.0 and 10.0 wt %, some encapsulation of the inner aqueous phase occurred within an amorphous PGPR oily outer phase (Figure 3h,i respectively). In the absence of PGPR, no MC structures were formed regardless of DOPC concentration. These results indicate that both DOPC and PGPR are required for MC assembly to occur. Presumably, PGPR plays a crucial stabilizing role, and DOPC plays a role in directing the structure. It is therefore likely that the hydrophobic layer is composed of both lipid and PGPR, forming hybrid hemi-fused compartments. To confirm,

https://doi.org/10.1021/acs.langmuir.2c02859
Langmuir 2023, 39, 4863−4871

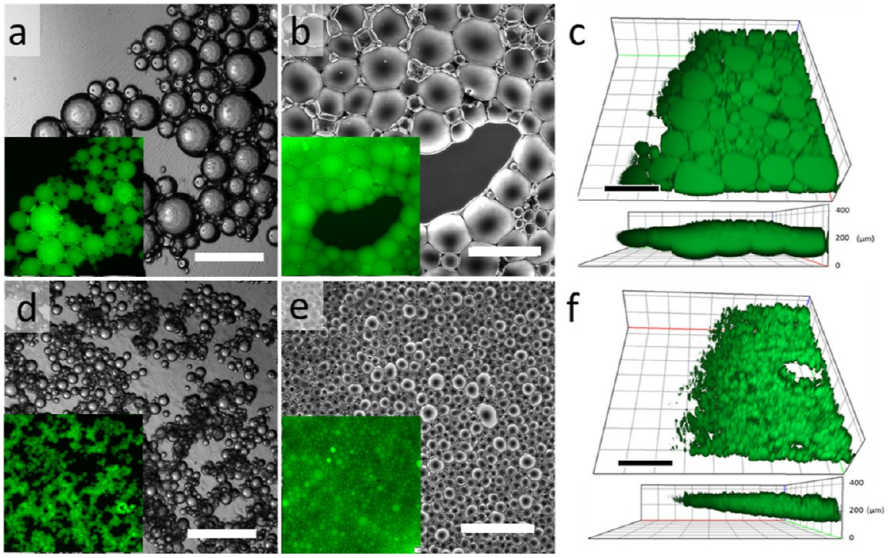

Figure 4. Aqueous droplets produced by calcein dye (100 μM) soaked lipid−MG sponge (lipid solution concentrations: DOPC 3.25 mM and PGPR 5 wt %) with (a) bright field and inset fluorescence images of droplets produced from placing MG sponge in hexane, (b) phase contrast and inset fluorescence images of droplets after hexane evaporation and droplet fusing, (c) 3D confocal images of post-hexane evaporation, with connected droplets showing tilted (upper) and side on (bottom) views, (d) bright field and inset fluorescence images of droplets produced from placing MG sponge in hexane and vortexing for 20 s after MG-sponge removal, (e) phase contrast and inset fluorescence images of vortexed droplets after hexane evaporation and droplet fusion, and (f) 3D confocal images of vortexed droplets post-hexane evaporation, showing tilted (upper) and side on (bottom) views. Scale bars represent 400 μm.

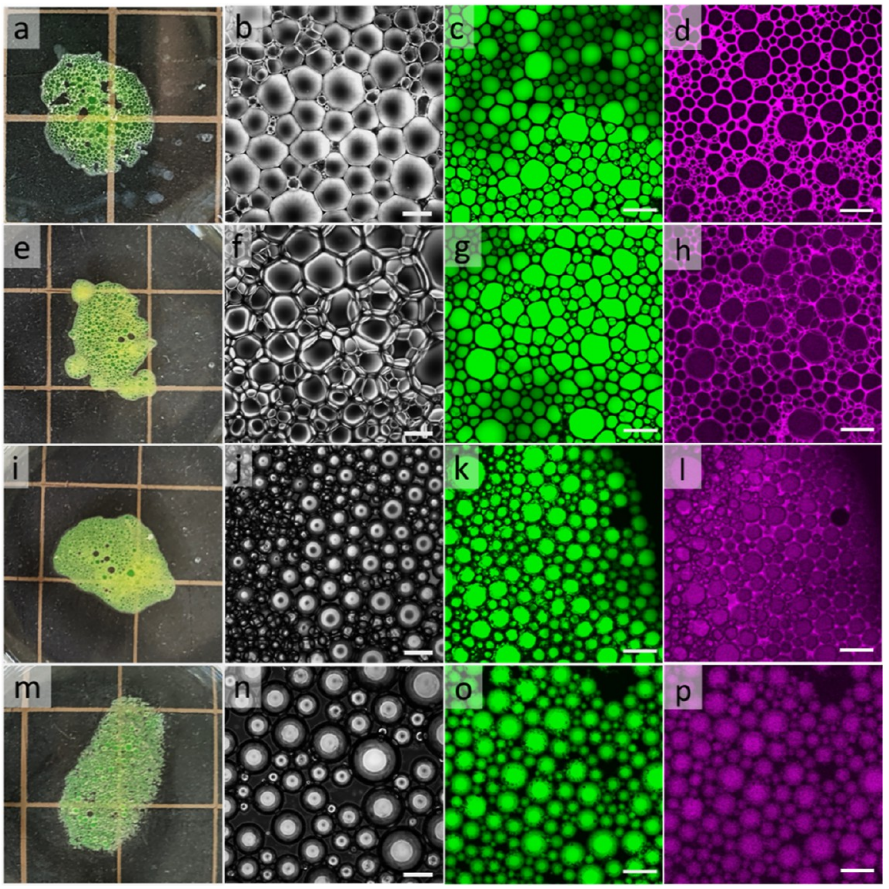

Figure 5. Images showing MC structures on macroscopic and microscopic scales with the addition of hexadecane oil of concentrations (a−d) 0 vol %, (e−h) 0.5 vol %, (i−l) 5.0 vol %, and (m−p) 100.0 vol %; (a,e,i,m) macroscopic scale images taken by a smartphone camera, where gridlines for the scale represent 1 cm^2; (b,f,j,n) phase contrast imaging with the scale bar of 200 μm, (c,g,k,o) confocal images at 473 nm showing aqueous calcein green, and (d,h,l,p) confocal images at 543 nm showing hydrophobic Nile red, where the scale bar of all confocal images represents 400 μm.

https://doi.org/10.1021/acs.langmuir.2c02859
Langmuir 2023, 39, 4863−4871

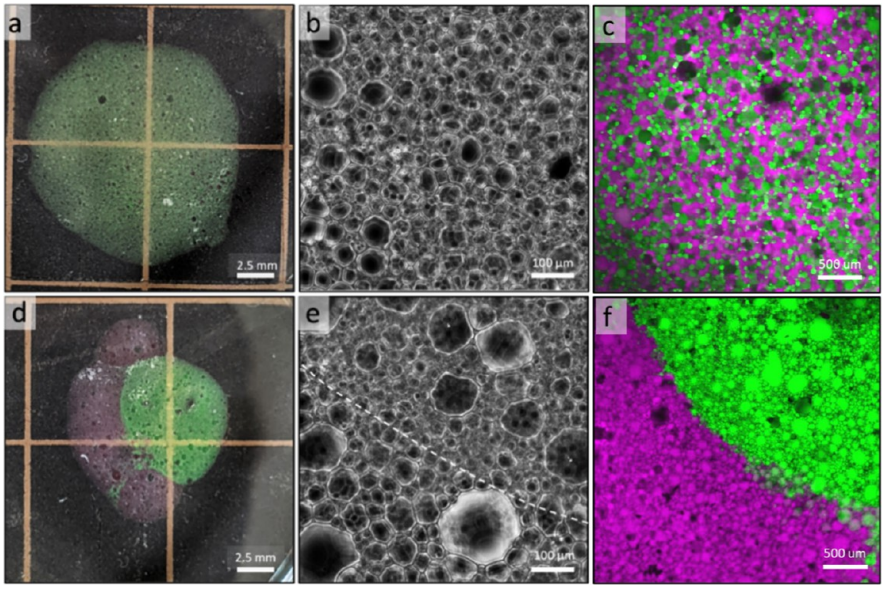

Figure 6. Heterogeneous MC structures containing calcein green and Dextran Texas Red filled compartments, whose macroscopic images, phase contrast images, and confocal microscopy images are shown from left to right, respectively, for (a,b,c) random distribution and (d,e,f) separated distribution of compartments.

the pore protein α-hemolysin was added into both the inner aqueous phase (absorbed into the MG sponge before compartment assembly) and the outer aqueous phase after MC assembly, neither of which resulted in the leakage of the internal calcein green dye into the external aqueous phase, nor was exchange or equilibration observed between compartments in heterogeneous systems containing sections with and without calcein green dye. This would fit with the idea of the lipid compartments being hemi-fused lipid-PGPR hybrid systems and not lipid bilayer membranes.

The mechanism of MC formation was investigated by observing the stabilized aqueous droplets before and after hexane oil evaporation. Aqueous calcein droplets formed from lipid-coated MG sponges (DOPC and PGPR concentrations of 3.25 mM and 5.0 wt %, respectively) were first observed by in the outer hexane solution by microscopy before pipetting onto the external aqueous solution and allowing evaporation to occur (Figure 4a). It was found that the size of the initial aqueous droplets in oil directly correlates to the size of the final tightly packed compartments. The preservation of size indicated that the assembled structure is simply made up of the initial droplets packed together (Figure 4b). After the loss of the carrier oil and assembly of the MC structure, the droplets are still floating on the surface of the water, as shown by the thin, single-compartment layer assembly on the external water surface (Figure 4c).

As it was expected that the flexibility of the membrane was essential to form the deformed, tightly packed structures, the effect of cholesterol, an additive known to "stiffen" DOPC lipid membranes, was investigated. Cholesterol added at 5 mol % relative to DOPC in the lipid solution was able to form stable droplets in oil; however, after transfer to the external water phase, it resulted in 90−100% catastrophic failure of the structure within seconds of the oil phase evaporating. This suggests that membrane flexibility is needed in MC formation.

The initial droplets were also tested for stability after vortexing. Vortexing calcein dye droplets in oil (w/o) for 20−30 s, the droplets were split into significantly smaller sizes (Figure 4d). Droplet stability in oil remained high after vortexing, and no size increase by coalescence is observed even after 24 h. After oil evaporation, MC structures formed from vortexed droplets show comparative structures with distorted lipid compartments in a tightly packed formation and complete encapsulation of inner aqueous liquids (Figure 4e). The diameter of the macroscopic structures however is increased for the same initial volume of aqueous "inner" liquid due to the reduction in height of the droplets (Figure 4f).

As it was suspected that the remaining oil would be partially dissolved into the lipid/PGPR hydrophobic layer after bulk oil evaporation, the role of oils on the structure was investigated. Hexane (high vapor pressure, fast evaporation) and hexadecane (low vapor pressure, slow evaporation) were chosen and used in different ratios for the oil phase used for droplet formation. Observation of the resulting structures after 60 min would then be expected to have a higher remaining oil content with higher concentrations of hexadecane. Figure 5a−d shows the formation of lipid-based compartments formed from only hexane oil. After the evaporation of hexane was observably complete, the compartments were well defined with a tightly packed structure. The distortion from an energetically favorable sphere is thought to come from hydrophobic forces minimizing the surface area contact with the external aqueous environment. With the addition of hexadecane in small amounts (0.5 vol % with respect to hexane), the structure remained largely the same as that of the purely hexane system, though some small differences occurred (Figure 5e−h). Figure 5f shows by phase contrast imaging that the structure may have additional build-up on the surface; however, by confocal microscopy, the observed slices of the hydrophilic inner compartments appeared identical to that of the hexane only system showing strained close packed compartments between 50 and 300 μm (Figure 5g). By imaging the hydrophobic lipid layers, however, it is observed that while the basic structure remained identical, the contrast between the lipid layer and the hydrophilic aqueous compartments was slightly reduced, and this would be expected in cases where the lipid layer is thicker

https://doi.org/10.1021/acs.langmuir.2c02859
Langmuir 2023, 39, 4863−4871

and the dye therefore more diffuse. As opposed to the hexane only oil from which the MC structures remain stable in the time scale of hours, with the addition of even 0.5 vol % hexadecane, the longevity of the structure increased to several days at room temperature conditions before any noticeable degradation occurred and up to approximately 2 weeks before catastrophic destruction of the structure occurred. The sharp increase in stability indicates the necessity of small amounts of oil in the hydrophobic lipid/PGPR layer. In the hexane only system, the relatively short life span (hours) could be explained by the gradual loss of residual hexane from the lipid layer. With further addition of hexadecane up to 5 vol % with respect to hexane, the connected lipid compartments become tightly packed but show spherical droplets. In this case, the larger volume of the oil phase increases the separation distance between the aqueous compartments and therefore allows the droplets to conform to a more relaxed spheroid shape (Figure 5i–l). The Nile red emission signal contrast between the outside hydrophobic lipid layer and the hydrophilic compartment is reduced further still. When hexadecane was used completely in place of hexane (hexadecane 100 vol %), the initial droplets did not form a tightly packed connected structure and the original separated water droplets in oil were maintained (Figure 5m,n). Interestingly, however, confocal microscopy revealed that the hydrophilic dyed and hydrophobic dyed sections completely overlapped (Figure 5o,p). This may indicate that the lipids are mostly or entirely coordinated to the aqueous droplets and not freely dispersed in the oil.

Heterogeneous assemblies of MC structures could also be assembled by adding aqueous droplets with different internal contents. Droplets of different types could be assembled in two different ways. First, two droplet types could be added together in the same oil mixture to create a randomly dispersed mixed system. The droplets in oil were found not to coalesce and mix their content but remained as separate droplets, which therefore preserved their heterogeneity. Figure 6a shows a macroscopic picture of a random mix heterogeneous MC structure with calcein and hydrophilic Dextran Texas Red-containing droplets. Phase contrast imaging (Figure 6b) did not reveal a difference in the structure, and the different droplets could therefore not be distinguished. Confocal microscopy with fluorescence imaging however revealed that the droplet contents were indeed separated with no dye overlap observed, and the mixture appeared random without any clustering, which indicated that the only difference is the internal aqueous content and it produced no effect on the stabilization by lipids or PGPR (Figure 6c). Second, the stabilized aqueous droplets in oil could be kept separate and sequentially pipetted onto the water surface to create sectionalized heterogeneous structures. Figure 6d shows the macroscopic result of sequentially combing droplets separately containing calcein and Texas Red, where the dye remains visibly spatially separated. Figure 6e shows the phase contrast image of the spatially separated MC structure with the separated droplet sections approximately given by the white dashed line on the figure (confirmed separately by fluorescence imaging), as with the random assembly, no structural difference is observed and the droplets cannot be distinguished. By confocal microscopy, however, a clear boundary between droplet types was observed (Figure 6f). Such heterogeneous systems may offer advantages in storing and transporting chemically incompatible species.

The hybrid lipid–oil compartment walls being thicker than bilayer membranes allows for the easy accommodation of hydrophobic nanoparticles in the lipid layer. Hydrophobic SPIONs modified with oleic acid (SPION-oleic) were added to the initial lipid solution at 1 mg mL^{-1} concentration, which could subsequently produce MC structures with magnetic response (Figure 7a). Figure 7b shows an MC structure

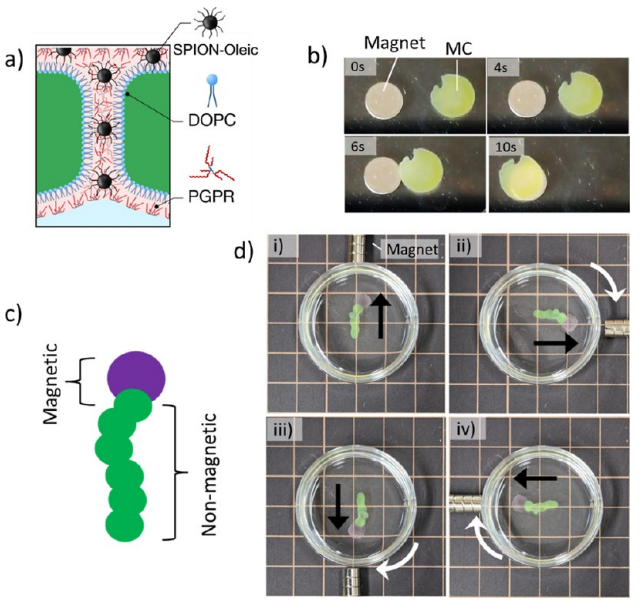

Figure 7. Magnetic MC structures showing (a) schematic for the location of oleic-modified SPIONs in the hydrophobic membrane of the MC structure and (b) magnetic MC structure (green) moving toward and over the neodymium magnet placed under the Petri dish. (c) Schematic of the heterogeneous magnetic MC structure with a magnetic head (purple) and a non-magnetic body (green) and (d) heterogeneous magnetic MC structure with a magnetic head (purple) and a non-magnetic body (green) turning in response to the neodymium magnet, where images (i–iv) are in a chronological sequence, black arrows point in the direction of the magnetic "head", and white arrows indicate the direction the structure has turned.

formed with SPION-oleic nanoparticles migrating toward a neodymium permanent magnet placed underneath the Petri dish, covering a 5 mm distance over 10 s. While the magnetic MC structure was able to migrate over the neodymium magnet while floating on the surface of water, magnetic strength was not sufficient to overcome the buoyancy and the magnet-MC structure remained on the water surface without any deformation, even while directly over the magnet. Combining SPION–oleic embedded compartments with non-magnetic compartments in spatially separated heterogeneous sections allowed for a level of directionality to be included in the MC structures. Figure 7c shows a schematic for a magnetically heterogeneous MC structure with a "magnetic head" connected to a non-magnetic body. While a magnetically homogeneous structure will migrate toward a permanent magnet without aligning to the field, magnetically heterogeneous structures will align to the magnetic field, adding a degree of directionality. Figure 7d(i–iv) shows a magnetically heterogeneous structure turning so that the magnetic head (seen as purple due to the inclusion of hydrophilic Texas Red dye) is facing toward a neodymium permanent magnet, and as the magnet is placed at 90° intervals around the circumference of the Petri dish, the magnet head turns to re-align to the

https://doi.org/10.1021/acs.langmuir.2c02859
Langmuir 2023, 39, 4863–4871

magnetic field. Over time, the heterogeneous structure also migrated toward the neodymium magnet, and so, the magnet was placed a further distance away to produce a weaker magnetic field and thereby prevent collision with the container wall. We predict that such separation and alignment may allow for more advanced manipulation of the structures with further work and using more sophisticated arrangements of heterogeneous systems. No morphological changes in the structure and no change in the stability or longevity of the structural integrity were observed with magnetic MC structures produced using hexane−hexadecane (hexadecane 0.5 vol % with respect to hexane), equally lasting for several days at room temperature conditions, comparable to structures without magnetic nanoparticles. In practical applications, the addition of magnetic response may allow for controlled motion of the structures. External manipulation of magnetic fields through permanent magnets or electromagnets would allow for a simple, non-harmful delivery of the aqueous solution-filled compartments and the contents therein as well as any hydrophobic species in the lipid−PGPR layer. Successful addition of magnetic nanoparticles may also indicate the possibility of including other hydrophobic nanomaterials such as polymers, clays, and colloids into the lipid layer, further extending their durability and utility.

CONCLUSIONS

We have discussed a method for producing centimeter-scale lipid-based "multicellular" compartmentalized structures, consisting of inner aqueous containers surrounded by hydrophobic lipid-based walls in a tightly packed structure. The MC structures were shown to require both PGPR, a commercial non-ionic surfactant, and the phospholipid DOPC for successful formation, indicating that the final form is a lipid−surfactant hybrid structure. While centimeter-sized structures were presented here, given suitable container sizes, it is believed that even larger sizes are achievable due to the ability of additive building of MCs. The longevity of the structures was found to be up to approximately 2 weeks before degradation of the structure starts, a time scale that would allow for many practical applications. The structures are effectively planar in form with a single layer of filled compartments floating on an outer aqueous solution. Due to the impermeable lipid hybrid walls, the contents remain separated even after joining together, and the retention of their starting internal composition after assembly allowed for creating structures of mixed droplet types. Mixing droplets containing different dyes resulted in observable heterogeneous structures, and it was shown that they could be added at the same time to form in a randomly mixed heterogeneous pattern or by sequential addition of droplet types, which allowed for the formation of spatially separated regions. This mixed, compartmentalized, and modular approach for heterogeneous structure formation could allow for the development of complex multifunctional materials from simple and scalable formations.

To demonstrate functionality, hydrophobic oleic acid-modified magnetic nanoparticles were added into the hybrid lipid layer, allowing for the structure to move in response to magnetic fields on a time scale of seconds, allowing real-time manipulation of motion. The ability to combine non-magnetic and magnetic sections in discrete sections allows for greater control, directionality, and steering of the MC structures, which may allow for future applications in the field of molecular robotics and soft robotics. We believe that the continued development of this work may lead to easier development and access of robust, biocompatible, multifunctional MC systems with a range of applications from soft robotics, microarrays, and cell-like models. Further to this, projects are also underway to enable molecular exchange and interactions in MC systems, enabling communication, memory, and learning.[23,24] MC systems presented here may provide a suitable structural basis for such molecular communication.

ASSOCIATED CONTENT

Supporting Information

The Supporting Information is available free of charge at https://pubs.acs.org/doi/10.1021/acs.langmuir.2c02859.

Phase contrast and fluorescence microscopy image of an MC structure formed from deionized H_2O without calcein green hydrophilic dye (PDF)

AUTHOR INFORMATION

Corresponding Authors

Richard J. Archer − *Molecular Robotics Laboratory, Department of Robotics, Graduate School of Engineering, Tohoku University, Sendai 980-8579, Japan;* orcid.org/0000-0003-2653-8207; Email: archer.richard.james.c8@tohoku.ac.jp

Shin-Ichiro M. Nomura − *Molecular Robotics Laboratory, Department of Robotics, Graduate School of Engineering, Tohoku University, Sendai 980-8579, Japan;* Email: shinichiro.nomura.b5@tohoku.ac.jp

Authors

Shogo Hamada − *Molecular Robotics Laboratory, Department of Robotics, Graduate School of Engineering, Tohoku University, Sendai 980-8579, Japan;* orcid.org/0000-0003-1910-0581

Ryo Shimizu − *Molecular Robotics Laboratory, Department of Robotics, Graduate School of Engineering, Tohoku University, Sendai 980-8579, Japan*

Complete contact information is available at: https://pubs.acs.org/10.1021/acs.langmuir.2c02859

Notes

The authors declare no competing financial interest.

ACKNOWLEDGMENTS

The authors thank Dr. Gen Hayase, Prof. Satoshi Murata, and Dr. Ibuki Kawamata for their constructive feedback. This work was supported by the JSPS/MEXT KAKENHI (grant numbers 20H05969, 22K12239, and 22H05396 to S.H. and 20H05701 "Project AutoMatter", 20H05970, and 20H00619 to S.M.N.).

REFERENCES

(1) Kaiser, D. Building a Multicellular Organism. *Annu. Rev. Genet.* **2001**, *35*, 103−123.

(2) Kin, K.; Schaap, P. Evolution of Multicellular Complexity in the Dictyostelid Social Amoebas. *Genes* **2021**, *12*, 487−502.

(3) Furusawa, C.; Kaneko, K. Origin of Complexity in Multicellular Organisms. *Phys. Rev. Lett.* **2000**, *84*, 6130−6133.

(4) Driscoll, W. W.; Travisano, M. Synergistic Cooperation Promotes Multicellular Performance and Unicellular Free-Rider Persistence. *Nat. Commun.* **2017**, *8*, 1−10.

(5) Chen, A. H.; Silver, P. A. Designing Biological Compartmentalization. *Trends Cell Biol.* **2012**, *22*, 662−670.
(6) Niklas, K. J.; Newman, S. A. The Origins of Multicellular Organisms. *Evol. Dev.* **2013**, *15*, 41−52.
(7) Agapakis, C. M.; Boyle, P. M.; Silver, P. A. Natural Strategies for the Spatial Optimization of Metabolism in Synthetic Biology. *Nat. Chem. Biol.* **2012**, *8*, 527−535.
(8) Nowak, M. A. Five Rules for the Evolution of Cooperation. *Science* **2006**, *314*, 1560−1563.
(9) Biernaskie, J. M.; West, S. A. Cooperation, Clumping and the Evolution of Multicellularity. *Proc. Biol. Sci.* **2015**, *282*, 20151075.
(10) Rueffler, C.; Hermisson, J.; Wagner, G. P. Evolution of Functional Specialization and Division of Labor. *Proc. Natl. Acad. Sci. U. S. A.* **2012**, *109*, E326−E335.
(11) Akbarzadeh, A.; Rezaei-sadabady, R.; Davaran, S.; Joo, S. W.; Zarghami, N.; Hanifehpour, Y.; Samiei, M.; Kouhi, M.; Kazem, N.-K. Liposome : Classification, Preparation, and Applications. *Nanoscale Res. Lett.* **2013**, *8*, 1−9.
(12) Rideau, E.; Dimova, R.; Schwille, P.; Wurm, F. R.; Landfester, K. Liposomes and Polymersomes: A Comparative Review towards Cell Mimicking. *Chem. Soc. Rev.* **2018**, *47*, 8572−8610.
(13) Walde, P.; Cosentino, K.; Engel, H.; Stano, P. Giant Vesicles: Preparations and Applications. *ChemBioChem* **2010**, *11*, 848−865.
(14) Hamada, T.; Yoshikawa, K. Cell-Sized Liposomes and Droplets: Real-World Modeling of Living Cells. *Materials* **2012**, *5*, 2292−2305.
(15) Hayase, G.; Nomura, S. I. M. Large-Scale Preparation of Giant Vesicles by Squeezing a Lipid-Coated Marshmallow-like Silicone Gel in a Buffer. *Langmuir* **2018**, *34*, 11021−11026.
(16) Inaba, H.; Uemura, A.; Morishita, K.; Kohiki, T.; Shigenaga, A.; Otaka, A.; Matsuura, K. Light-Induced Propulsion of a Giant Liposome Driven by Peptide Nanofibre Growth. *Sci. Rep.* **2018**, *8*, 2−11.
(17) Čejková, J.; Banno, T.; Hanczyc, M. M.; Štěpánek, F. Droplets As Liquid Robots. *Artif. Life* **2017**, *23*, 528−549.
(18) Hanczyc, M. M.; Toyota, T.; Ikegami, T.; Packard, N.; Sugawara, T. Fatty Acid Chemistry at the Oil-Water Interface: Self-Propelled Oil Droplets. *J. Am. Chem. Soc.* **2007**, *129*, 9386−9391.
(19) Matsuo, M.; Ohyama, S.; Sakurai, K.; Toyota, T.; Suzuki, K.; Sugawara, T. A Sustainable Self-Reproducing Liposome Consisting of a Synthetic Phospholipid. *Chem. Phys. Lipids* **2019**, *222*, 1−7.
(20) Hayashi, M.; Nishiyama, M.; Kazayama, Y.; Toyota, T.; Harada, Y.; Takiguchi, K. Reversible Morphological Control of Tubulin-Encapsulating Giant Liposomes by Hydrostatic Pressure. *Langmuir* **2016**, *32*, 3794−3802.
(21) Sato, Y.; Hiratsuka, Y.; Kawamata, I.; Murata, S.; Nomura, S. I. M. Micrometer-Sized Molecular Robot Changes Its Shape in Response to Signal Molecules. *Sci. Rob.* **2017**, *2* (). https://doi.org/DOI: 10.1126/scirobotics.aal3735.
(22) Bayoumi, M.; Bayley, H.; Maglia, G.; Sapra, K. T. Multi-Compartment Encapsulation of Communicating Droplets and Droplet Networks in Hydrogel as a Model for Artificial Cells. *Sci. Rep.* **2017**, *7*, 1−11.
(23) Zhou, K.; Tian, T.; Wang, C.; Zhao, H.; Gao, N.; Yin, H.; Wang, P.; Ravoo, B. J.; Li, G. Multifunctional Integrated Compartment Systems for Incompatible Cascade Reactions Based on Onion-Like Photonic Spheres. *J. Am. Chem. Soc.* **2020**, *142*, 20605−20615.
(24) Gröschel, A. H.; Müller, A. H. E. Self-Assembly Concepts for Multicompartment Nanostructures. *Nanoscale* **2015**, *7*, 11841−11876.
(25) Aufinger, L.; Simmel, F. C. Establishing Communication Between Artificial Cells. *Chem.—Eur. J.* **2019**, *25*, 12659−12670.
(26) Murata, S.; Toyota, T.; Nomura, S.; Nakakuki, T.; Kuzuya, A. Molecular Cybernetics: Challenges toward Cellular Chemical AI. *Adv. Funct. Mater.* **2022**, *32*, 2201866.
(27) Trantidou, T.; Friddin, M. S.; Salehi-Reyhani, A.; Ces, O.; Elani, Y. Droplet Microfluidics for the Construction of Compartmentalised Model Membranes. *Lab Chip* **2018**, *18*, 2488−2509.
(28) Song, Y.; Jiang, R.; Wang, Z.; Yin, Y.; Li, B.; Shi, A. C. Formation and Regulation of Multicompartment Vesicles from Cyclic Diblock Copolymer Solutions: A Simulation Study. *ACS Omega* **2020**, *5*, 9366−9376.
(29) Oda, A.; Watanabe, C.; Aoki, N.; Yanagisawa, M. Liposomal Adhesion: Via Electrostatic Interactions and Osmotic Deflation Increase Membrane Tension and Lipid Diffusion Coefficient. *Soft Matter* **2020**, *16*, 4549−4554.
(30) Estes, D. J.; Lopez, S. R.; Fuller, A. O.; Mayer, M. Triggering and Visualizing the Aggregation and Fusion of Lipid Membranes in Microfluidic Chambers. *Biophys. J.* **2006**, *91*, 233−243.
(31) Bolognesi, G.; Friddin, M. S.; Salehi-Reyhani, A.; Barlow, N. E.; Brooks, N. J.; Ces, O.; Elani, Y. Sculpting and Fusing Biomimetic Vesicle Networks Using Optical Tweezers. *Nat. Commun.* **2018**, *9*, 1−11.
(32) Elani, Y.; Gee, A.; Law, R. V.; Ces, O. Engineering Multi-Compartment Vesicle Networks. *Chem. Sci.* **2013**, *4*, 3332−3338.
(33) Villar, G.; Graham, A. D.; Bayley, H. A Tissue-Like Printed Material. *Science* **2013**, *340*, 48−52.
(34) Villar, G.; Heron, A. J.; Bayley, H. Formation of Droplet Networks That Function in Aqueous Environments. *Nat. Nanotechnol.* **2011**, *6*, 803−808.
(35) Booth, M. J.; Schild, V. R.; Downs, F. G.; Bayley, H. Functional Aqueous Droplet Networks. *Mol. Biosyst.* **2017**, *13*, 1658−1691.
(36) Czekalska, M. A.; Jacobs, A. M. J.; Toprakcioglu, Z.; Kong, L.; Baumann, K. N.; Gang, H.; Zubaite, G.; Ye, R.; Mu, B.; Levin, A.; Huck, W. T. S.; Knowles, T. P. J. One-Step Generation of Multisomes from Lipid-Stabilized Double Emulsions. *ACS Appl. Mater. Interfaces* **2021**, *13*, 6739−6747.
(37) Elani, Y.; Law, R. V.; Ces, O. Vesicle-Based Artificial Cells as Chemical Microreactors with Spatially Segregated Reaction Pathways. *Nat. Commun.* **2014**, *5*. https://doi.org/ DOI: 10.1038/ncomms6305.
(38) Downs, F. G.; Lunn, D. J.; Booth, M. J.; Sauer, J. B.; Ramsay, W. J.; Klemperer, R. G.; Hawker, C. J.; Bayley, H. Multi-Responsive Hydrogel Structures from Patterned Droplet Networks. *Nat. Chem.* **2020**, *12*, 363−371.
(39) Nomura, S. M.; Shimizu, R.; Archer, R. J.; Hayase, G.; Toyota, T.; Mayne, R.; Adamatzky, A. Spontaneous and Driven Growth of Multicellular Lipid Compartments to Millimeter Size from Porous Polymer Structures. *ChemSystemsChem* **2022**, *4*, 202200006.
(40) Hayase, G.; Kanamori, K.; Fukuchi, M.; Kaji, H.; Nakanishi, K. Facile Synthesis of Marshmallow-like Macroporous Gels Useable under Harsh Conditions for the Separation of Oil and Water. *Angew. Chem., Int. Ed.* **2013**, *52*, 1986−1989.
(41) Lobato, N. C. C.; Mansur, M. B.; Ferreira, A. Characterization and Chemical Stability of Hydrophilic and Hydrophobic Magnetic Nanoparticles. *Mater. Res.* **2017**, *20*, 736−746.

https://doi.org/10.1021/acs.langmuir.2c02859
Langmuir 2023, 39, 4863−4871